Journal Pre-proofs

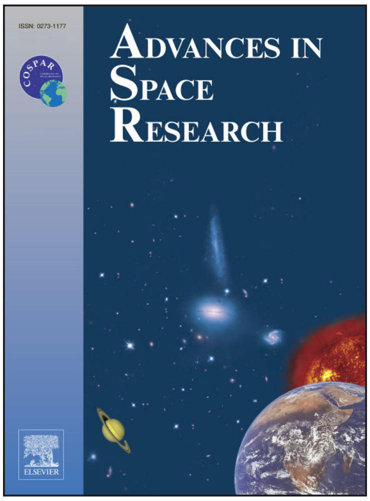


Detumbling of axisymmetric space debris during transportation by ion beam shepherd in 3D case

Vladimir Aslanov, Alexander Ledkov

PII: S0273-1177(21)00762-6
DOI: https://doi.org/10.1016/j.asr.2021.10.002
Reference: JASR 15538

To appear in: *Advances in Space Research*

Received Date: 1 June 2021
Revised Date: 3 September 2021
Accepted Date: 1 October 2021

# Detumbling of axisymmetric space debris during transportation by ion beam shepherd in 3D case

Vladimir Aslanov[1], Alexander Ledkov

Samara National Research University, 34, Moscovskoe shosse, Samara 443086, Russia

**Abstract**

The paper considers the contactless transportation of space debris by means of an ion beam generated by an active spacecraft electrodynamic engine. The three-dimensional motion of a space debris object relative to its center of mass is studied. Space debris is assumed to be a dynamically symmetric cylindrical rigid body. The aim of the paper is to develop a control of the engine thrust, which ensures the stabilization of spatial oscillations of cylindrical space debris. A simplified mathematical model describing the motion of a dynamically symmetric rigid body in a Keplerian orbit is developed. For the case of a circular orbit, stationary motions relative to the center of mass are found. A feedback control law for the thrust of an electrodynamic engine creating an ion beam, which is aimed at stabilizing the space debris object in a stationary angular position, is proposed. The results of numerical research confirm the effectiveness of this control. The research results can be used in the preparation of space debris removal missions.

Keywords: Ion beam shepherd; space debris; removal mission; detumbling; control law

[1] Corresponding author
*E-mail address*: aslanov_vs@mail.ru

# 1. Introduction

Developing of active space debris removal systems is one of the most important challenges facing the space industry today. Despite the fact that the problem has been actively discussed by the scientific community for several decades (Bonnal and Alby, 2000; Klinkrad et al., 2004; Shan et al., 2016), the situation with space debris in orbit continues to deteriorate (NASA, 2021). Back in 1978, a dramatic scenario in which collisions of large space debris could trigger a chain reaction that would exponentially increase the flow of space debris and make it impossible to use orbits was described (Kessler and Cour-Palais, 1978). In 2009, the collision of Cosmos 2251 and Iridium 33 led to the formation of clouds of debris, some of which will remain in orbit until 2090 (Pardini and Anselmo, 2011). For space debris objects, various indexes are proposed, reflecting their potential hazard based on an analysis of various factors (Letizia et al., 2019; Pardini and Anselmo, 2020; Rossi et al., 2015). These indices allow selecting the objects to be removed first. The growth of the population of space debris leads to the complication of the operating conditions of space vehicles. T. Maclay and D. McKnight propose "Space Environment Management" concept, consisting of both debris mitigation and debris remediation, as response to growing threat to space safety (Maclay and McKnight, 2021). Currently, a large number of various active space debris removal projects are actively discussed in the scientific literature (Mark and Kamath, 2019). All these projects can be conditionally divided into three groups: systems involving docking/capturing and hard mechanical contact of an active spacecraft-cleaner and passive space debris object (Baranov et al., 2021; Hakima and Emami, 2021); systems involving remote capture and subsequent transportation of a space debris object on a tether (Aslanov, 2016; Zhong and Zhu, 2016); and systems that do not involve direct mechanical contact. The main advantage of contactless transportation systems is their safety. The absence of mechanical contact reduces the risk of an accident when capturing space debris. In addition, contactless methods can be used to space debris detumbling, which is critical for the first two contact transport methods (Bennett and Schaub, 2018; Nakajima et al., 2018; Yu et al., 2021).

Contactless transportation of a space debris object can be performed in various ways. Space based lasers can be used for this purpose (Ivakin et al., 2019; Peltoniemi et al., 2021). The transfer of force to a passive space debris object can be carried out by means of electromagnetic (Yu et al., 2021), electrostatic (Schaub and Moorer, 2012) or gravitational fields (Aslanov, 2019). Another promising method is the use of an ion beam generated by the electrodynamic thruster of an active spacecraft. Hitting into the surface of space debris, ions transfer their impulse to it, thus generating a force impact. This ion beam space debris removal scheme was proposed independently by C. Bombardelli and J. Pelaez (Bombardelli and Peláez, 2011) and S. Kitamura (Kitamura, 2010; Kitamura et al., 2014). The motion of a passive object of space debris during its contactless transportation by an ion beam is considered in this study. The concept "Ion Beam Shepherd", which was developed by the team LEOSWEEP under the FP grant (Alpatov et al., 2019), is taken as a basis.

To date, the process of contactless space debris removal by an ion beam without taking into account the motion of space debris relative to the center of mass is investigated in detail (Bombardelli and Peláez, 2011; Cichocki et al., 2017). The control law of an active spacecraft (Alpatov et al., 2018; Khoroshylov, 2020), and methods for choosing the parameters of a space debris removal mission using an ion beam are proposed (Urrutxua et al., 2019). Optimization of the mission of sequential deorbiting of several space debris objects and optimization of the parameters of a spacecraft based on the Express-1000NV platform are considered in (Obukhov et al., 2021). The influence of angular oscillations of cylindrical space debris object on the transportation process in the planar case is studied in papers (Aslanov et al., 2020; Aslanov and Ledkov, 2017). Several control laws for the ion velocity and ion beam axis direction, which are aimed at stabilizing the angular oscillations of space debris object, are proposed in (Aslanov and Ledkov, 2020) for the planar case of motion. It is shown that the angular mode of motion has a noticeable effect on the time taken to remove space debris from orbit (Aslanov and Ledkov, 2017), and that control of the angular oscillations of space debris can lead to noticeable fuel savings (Popov et al., 2020). The control algorithm for space debris detumbling in spatial case is proposed in (Nakajima et al., 2018).The planar case of motion is ideal, it is not realizable in practice due to the presence of external disturbances. Therefore, of practical interest is primarily the spatial case of the motion of space debris relative to the center of mass.

Previous studies have shown that in the case of planar motion, the transport of space debris in the equilibrium position is more efficient in terms of minimizing the space debris removal time than in the case of oscillations (Aslanov and Ledkov, 2017; Popov et al., 2020). The purpose of this work is to develop a control of the engine thrust, which ensures the stabilization of spatial oscillations of cylindrical space debris. To achieve this goal a mathematical model of the space debris and active spacecraft 3D motion is developed in this study. A stationary mode of angular oscillations under the action of gravitational and ion torques in the case of unperturbed motion of the space debris center of mass in a circular orbit is found. A feedback control law that transfers space debris to the stationary mode is proposed. Numerical simulations and analysis are performed.

## 2. Mathematical model

A mechanical system consisting of a space debris object and an active spacecraft (ion beam shepherd) is considered in this study. The space debris is a rigid body with a shape close to a cylinder. Many satellites and rocket stages have this shape. An active spacecraft is a material point. In addition to the main propulsion system, this spacecraft is equipped with a low thrust electrodynamic engine that creates an ions flow to transfer a force on the surface of the space debris object. These force and torque will be referred to below as ion force and ion torque. It is assumed that the system motion occurs under the action of gravitational forces and torques, the thrust force of the active spacecraft's engines, as well as the force and torque generated by the ion beam on the space debris surface.

The study requires the definition of multiple coordinate systems shown in Fig.1. The origin of the planetocentric frame $OX_pY_pZ_p$ is the center of the Earth. The axis $OY_p$ is directed along the Earth's rotation axis. Axes $OX_p$ and $OZ_p$ lie in the equatorial plane. This coordinate system is inertial. The origin of the orbital reference frame $BX_oY_oZ_o$ coincides with the center of mass of the space debris object. The axis $BZ_o$ the axis is directed from the center of the Earth to the spacecraft center of mass, the axis $BX_o$ is parallel to the plane $OX_pZ_p$ and it is directed towards the orbital flight, the axis $BY_o$ completes the right-hand triad. Transformation from planetocentric frame $OX_pY_pZ_p$ to orbital frame $BX_oY_oZ_o$ can be performed by two rotations: the positive rotation around the axis $OY_p$ on the angle $f$, and the negative rotation (clockwise) around the axis $OX_o$ on the angle $\nu$(Fig.1). It should be noted that $BX_oY_oZ_o$ is different from the conventional orbital reference frame, which requires one more rotation in order to direct $BX_o$ axis tangentially to the orbit. The axes of the body frame $BX_bY_bZ_b$ are principal body axes. The orientation of the body frame relative to the orbital frame can be specified by three Euler angles $\gamma$ , $\theta$, and $\varphi$ (rotation sequences is xzx). The reference frame $BX_oY_1Z_1$ shown in the Fig. 1 is obtained by rotating the orbital frame $BX_oY_oZ_o$ by $\gamma$ angle about $BX_o$ axis.

To translate the coordinates of a vector from one coordinate system to another, rotation matrices are used

$$\mathbf{r}^i = \mathbf{M}_{ij}\mathbf{r}^j,$$

where $\mathbf{r}^i$ is a vector given by its coordinates in the $i$-th coordinate system, $\mathbf{r}^j$ is a vector given by its coordinates in the $j$-th coordinate system, $\mathbf{M}_{ij}$ is the rotation matrix, which provides transformation from $j$-th frame to $i$-th frame. The superscripts of the vectors are used to indicate the coordinate system in which their

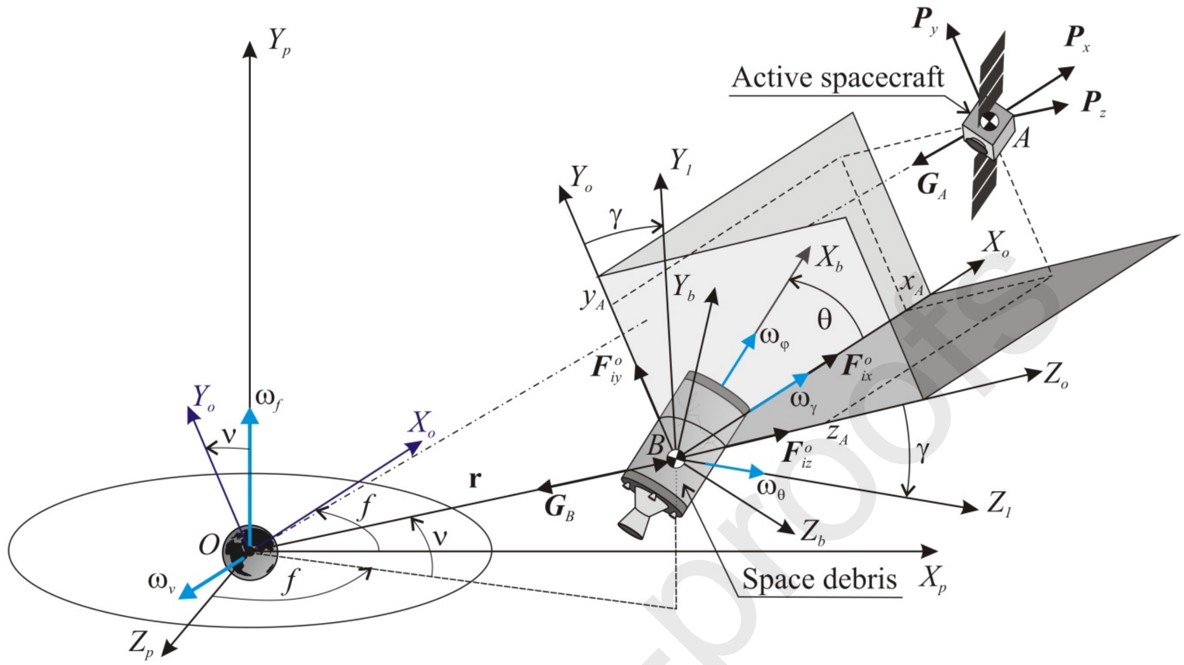


Fig. 1. Mechanical system and reference frames.

components are specified. All rotation matrices and detailed description of reference frames used in this study are given in the appendix.

### 2.1 Equations of translational 3D motion

The motion of the active spacecraft and the center of mass of the space debris can be described by Newton's law

$$m_A \ddot{\mathbf{r}}_A^p = \mathbf{G}_A^p + \mathbf{P}^p, \tag{2}$$

$$m_B \ddot{\mathbf{r}}_B^p = \mathbf{G}_B^p + \mathbf{F}_I^p, \tag{3}$$

where $m_A$, $m_B$ are the mass of the spacecraft and the space debris object, $\mathbf{r}_j$ is the position vectors of $j$-th point, the superscript $p$ indicates that the vectors are in the planetocentric frame $OX_pY_pZ_p$, $\mathbf{G}_j^p = -\frac{\mu m_j}{r_j^3}\mathbf{r}_j^p$ is the gravitational force acting on $j$-th point, $\mu$ is gravitational constant of the Earth, $\mathbf{P}$ is the total thrust of the



Journal Pre-proofs

active spacecraft's engines, $\mathbf{F}_I$ is the ion beam force. It is assumed that the thrust force and ion beam force are given by its components in the orbital frame $BX_oY_oZ_o$

$$\mathbf{P}^o = [P_x, P_y, P_z]^T, \qquad \mathbf{F}_I^o = [F_{ix}^o, F_{iy}^o, F_{iz}^o]^T. \tag{4}$$

The rotation matrix $\mathbf{M}_{po}$ given in the appendix is used to convert these vectors to the coordinate system $OX_pY_pZ_p$:

$$\mathbf{P}^p = \mathbf{M}_{po}\mathbf{P}^o, \qquad \mathbf{F}_I^p = \mathbf{M}_{po}\mathbf{F}_I^o. \tag{5}$$

The position vector of the active spacecraft can be found as the sum

$$\mathbf{r}_A^p = \mathbf{r}_B^p + \boldsymbol{\rho}^p = \mathbf{r}_B^p + \mathbf{M}_{po}\boldsymbol{\rho}^o, \tag{6}$$

where $\boldsymbol{\rho}^o = [x_A, y_A, z_A]^T$ is the spacecraft's position vector in orbital coordinate frame, $\mathbf{r}_B^p$ is the space debris center of mass position vector, which has following components in $OX_pY_pZ_p$

$$\mathbf{r}_B^p = [r\sin f\cos\nu,\ r\sin\nu,\ r\cos f\cos\nu]^T. \tag{7}$$

Substitution of (6) into (2) and expression of the second derivatives $\ddot{x}_A$, $\ddot{y}_A$, $\ddot{z}_A$ from the projections of (20) gives

$$\begin{aligned}
\ddot{x}_A &= -\frac{\mu x_A}{r_A^3} + \frac{P_x}{m_A} + (y_A\sin\nu - (r+z_A)\cos\nu)\ddot{f} + \dot{f}^2 x_A + 2\dot{f}\big((\dot{\nu}y_A - \dot{r} - \dot{z}_A)\cos\nu \\
&\quad + ((r+z_A)\dot{\nu} + \dot{y}_A)\sin\nu\big), \\
\ddot{y}_A &= -\frac{\mu y_A}{r_A^3} + \frac{P_y}{m_A} - x_A\ddot{f}\sin\nu - (r+z_A)\ddot{\nu} + y_A\dot{\nu}^2 - 2\dot{x}_A\dot{f}\sin\nu - 2(\dot{z}_A + \dot{r})\dot{\nu} \\
&\quad + (y_A\sin\nu - (r+z_A)\cos\nu)\dot{f}^2\sin\nu, \\
\ddot{z}_A &= -\frac{\mu(r+z_A)}{r_A^3} + \frac{P_z}{m_A} - \ddot{r} + x_A\ddot{f}\cos\nu + y_A\ddot{\nu} + (r+z_A)\dot{\nu}^2 + 2\dot{y}_A\dot{\nu} + 2x_A\dot{f}\cos\nu \\
&\quad - (y_A\sin\nu - (r+z_A)\cos\nu)\dot{f}^2\cos\nu.
\end{aligned} \tag{8}$$

Calculating the derivatives and solving equation (3) for the second derivatives yields

$$\ddot{r} = r(\dot{v}^2 + \dot{f}^2 \cos v^2) - \frac{\mu}{r^2} + \frac{F^o_{iz}}{m_B},$$
$$\ddot{f} = \frac{2\dot{f}\dot{v}s_v}{\cos v} - \frac{2\dot{f}\dot{r}}{r} + \frac{F^o_{ix}}{rm_B \cos v}, \tag{9}$$
$$\ddot{v} = -\dot{f}^2 \sin v \cos v - \frac{2\dot{v}\dot{r}}{r} + \frac{F^o_{iy}}{rm_B}.$$

Equations (8) and (9) describe the motion of the centers of mass of the considered mechanical system elements. The ion force projections on the right-hand side of equations (9) depend on the orientation of the space debris object in the ion beam; therefore, the system of equations (8) - (9) should be supplemented with equations of the space debris attitude motion.

### 2.2 Equations of the space debris attitude 3D motion

The attitude motion of the space debris object can be describes using Euler's equations (Schaub and Junkins, 2014)

$$\frac{d\mathbf{H}^b_B}{dt} + \boldsymbol{\omega}^b \times \mathbf{H}^b_B = \mathbf{L}^b_G + \mathbf{L}^b_I \ , \tag{10}$$

where $\mathbf{H}^b_B = [\mathbf{I}]\boldsymbol{\omega}^b$ is the angular momentum vector about the space debris object center of mass $B$, $\boldsymbol{\omega}^b = [\omega_x, \omega_y, \omega_z]^T$ is the space debris angular velocity, $[\mathbf{I}]$ is the inertia matrix, $\mathbf{L}^b_G$ is the gravity gradient torque, $\mathbf{L}^b_I = [L_{Ix}, L_{Iy}, L_{Iz}]^T$ is the ion beam torque relative to the center of mass of the space debris. All vectors are given by their components in the body reference frame.

The angular velocity vector $\boldsymbol{\omega}^b$ is the sum of the angular velocity vectors

$$\boldsymbol{\omega}^b = \boldsymbol{\omega}^b_v + \boldsymbol{\omega}^b_f + \boldsymbol{\omega}^b_\gamma + \boldsymbol{\omega}^b_\theta + \boldsymbol{\omega}^b_\varphi = \mathbf{M}_{bo}\boldsymbol{\omega}^o_v + \mathbf{M}_{bp}\boldsymbol{\omega}^p_f + \mathbf{M}_{bo}\boldsymbol{\omega}^o_\gamma + \boldsymbol{\omega}^b_\theta + \boldsymbol{\omega}^b_\varphi, \tag{11}$$

where $\boldsymbol{\omega}^o_v = [-\dot{v}, 0, 0]^T$, $\boldsymbol{\omega}^p_f = [0, \dot{f}, 0]^T$, $\boldsymbol{\omega}^o_\gamma = [\dot{\gamma}, 0, 0]^T$, $\boldsymbol{\omega}^b_\theta = [0, \dot{\theta}\sin\varphi, \dot{\theta}\cos\varphi]^T$, $\boldsymbol{\omega}^b_\varphi = [\dot{\varphi}, 0, 0]^T$, the rotation matrices $\mathbf{M}_{ij}$ are given in the appendix. Transferring all vectors to the body coordinate system, from (9) it follows

$$\boldsymbol{\omega}^b = \begin{bmatrix} \dot{\varphi} + \dot{\gamma} c_\theta - \dot{\nu} c_\theta + \dot{f}(c_\nu s_\theta c_\gamma + s_\nu s_\theta s_\gamma) \\ \dot{\theta} s_\varphi - \dot{\gamma} s_\theta c_\varphi + \dot{\nu} c_\varphi s_\theta + \dot{f}(c_\nu (c_\varphi c_\theta c_\gamma - s_\varphi s_\gamma) + s_\nu (s_\varphi c_\gamma + c_\varphi c_\theta s_\gamma)) \\ \dot{\theta} c_\varphi + \dot{\gamma} s_\theta s_\varphi - \dot{\nu} s_\varphi s_\theta + \dot{f}(-c_\nu (s_\varphi c_\theta c_\gamma + c_\varphi s_\gamma) + s_\nu (c_\varphi c_\gamma - s_\varphi c_\theta s_\gamma)) \end{bmatrix}, \tag{12}$$

where $c_\alpha = \cos\alpha$, $s_\alpha = \sin\alpha$.

The gravity gradient torque is given by the equation (Schaub and Junkins, 2014)

$$\mathbf{L}_G^b = \frac{3\mu}{r^5} \mathbf{r}^b \times [\mathbf{I}] \mathbf{r}^b = \frac{3\mu}{r^3} \begin{bmatrix} (I_z - I_y)\overline{r}_y \overline{r}_z \\ (I_x - I_z)\overline{r}_x \overline{r}_z \\ (I_y - I_x)\overline{r}_x \overline{r}_y \end{bmatrix}, \tag{13}$$

where center of mass vector $\mathbf{r}^b = \mathbf{M}_{bo}[0\ 0\ r]^T = r[\overline{r}_x\ \overline{r}_y\ \overline{r}_z]^T$, $I_x$, $I_y$, $I_z$ are principle moments of inertia of the space debris object. Equation (10) can be reduced to

$$\begin{aligned} \dot{\omega}_x &= \frac{I_y - I_z}{I_x}\left(\omega_y \omega_z - \frac{3\mu}{r^3}\overline{r}_y \overline{r}_z\right) + \frac{L_{Ix}}{I_x}, \\ \dot{\omega}_y &= \frac{I_z - I_x}{I_y}\left(\omega_x \omega_z - \frac{3\mu}{r^3}\overline{r}_x \overline{r}_z\right) + \frac{L_{Iy}}{I_y}, \\ \dot{\omega}_z &= \frac{I_x - I_y}{I_z}\left(\omega_x \omega_y - \frac{3\mu}{r^3}\overline{r}_x \overline{r}_y\right) + \frac{L_{Iz}}{I_z}. \end{aligned} \tag{14}$$

Equations (12), (14) describe the attitude motion of the space debris object under the action of the gravitational and the ion beam torques.

### 2.3 Equations of a symmetrical space debris attitude motion in R-G variables

Consider the case of motion of a symmetrical space debris object. It is assumed that $I_y = I_z = I$, and the center of mass of the space debris moves in a plane $\nu = 0$, $\dot{\nu} = 0$. Following the approach described in the book (Aslanov, 2017), new variables are introduced based on the classical Lagrange case of motion of a body with a fixed point. In the Lagrange case the generalized momentum corresponding to rotation and precession angles are integrals of motion. In the case of perturbed motion, these quantities will be slowly changing functions

$$R = \bar{I}_x \omega_x, \qquad G = R\cos\theta + (\omega_z \sin\varphi - \omega_y \cos\varphi)\sin\theta, \tag{15}$$

where $\bar{I}_x = I_x / I$. Expression the angular velocities from (12) and (15) gives

$$\begin{aligned}
\omega_x &= \frac{R}{\bar{I}_x}, \\
\omega_y &= \dot{\theta} s_\varphi - \frac{(G - Rc_\theta)c_\varphi}{s_\theta} - \dot{f} s_\varphi (c_\nu s_\gamma - s_\nu c_\gamma), \\
\omega_z &= \dot{\theta} c_\varphi + \frac{(G - Rc_\theta)s_\varphi}{s_\theta} - \dot{f} c_\varphi (c_\nu s_\gamma - s_\nu c_\gamma),
\end{aligned} \tag{16}$$

$$\dot{\gamma} = \frac{G - Rc_\theta}{s_\theta^2} + \dot{\nu} + \frac{\dot{f} c_\theta (c_\nu c_\gamma + s_\nu s_\gamma)}{s_\theta}, \tag{17}$$

$$\dot{\varphi} = \frac{R}{\bar{I}_x} - \frac{(G - Rc_\theta)c_\theta}{s_\theta^2} - \frac{\dot{f}(c_\nu c_\gamma + s_\nu s_\gamma)}{s_\theta}. \tag{18}$$

After substituting equations (16) in (14), expressing the derivatives yields

$$\ddot{f} = -\frac{2\dot{f}\dot{r}}{r} + \frac{F_{ix}^o}{r m_B}, \quad \ddot{r} = \dot{f}^2 r - \frac{\mu}{r^2} + \frac{F_{iz}^o}{m_B}. \tag{19}$$

$$\dot{\gamma} = \frac{G - R\cos\theta}{\sin^2\theta} + \frac{\dot{f}\cos\theta\cos\gamma}{\sin\theta}, \tag{20}$$

$$\dot{\varphi} = \frac{R}{\bar{I}_x} - \frac{(G - R\cos\theta)\cos\theta}{\sin^2\theta} - \frac{\dot{f}\cos\gamma}{\sin\theta}. \tag{21}$$

$$\begin{aligned}
\ddot{\theta} + \frac{(G - R\cos\theta)(R - G\cos\theta)}{\sin^3\theta} &= \frac{\dot{f}^2\cos^2\gamma\cos\theta}{\sin\theta} \\
+ \frac{2\dot{f}\cos\gamma(G - R\cos\theta)}{\sin^2\theta} &+ \frac{L_I}{I} - \frac{3\mu\sin^2\gamma\cos\theta\sin\theta(I_x - I)}{r^3 I},
\end{aligned} \tag{22}$$

$$\dot{R} = 0, \tag{23}$$

$$\begin{aligned}
\dot{G} = &\frac{\dot{f}\sin\gamma(G\cos\theta - R)}{\sin\theta} + \dot{f}^2\cos\gamma\sin\gamma - \dot{\theta}\dot{f}\cos\gamma \\
&- \frac{3\mu\cos\gamma\sin\gamma\sin^2\theta(I_x - I)}{r^3 I},
\end{aligned} \tag{24}$$

where $L_I = L_{Iz}\cos\varphi + L_{Iy}\sin\varphi$ is the projection of the ion torque on the $BZ_2$ axis of $BX_bY_3Z_2$ frame, which is described in the appendix. In the case of an axisymmetric body, $L_I$ projection does not depend on the angle $\varphi$.

Consider the case when the center of mass moves in an elliptical orbit.

$$r = \frac{p}{1+e\cos f}, \qquad \dot{f} = n(1+e\cos f)^2, \tag{25}$$

where $n = \sqrt{\mu a^{-3}}$, $a$ is the length of the semi-major axis of the orbit. The motion of space debris relative to the center of mass is determined by the equations

$$\begin{aligned}\ddot{\theta} + \frac{(G-R\cos\theta)(R-G\cos\theta)}{\sin^3\theta} = \frac{L_I}{I} + \frac{n^2(1+e\cos f)^4\cos^2\gamma\cos\theta}{\sin\theta}\\ + \frac{2n(1+e\cos f)^2\cos\gamma(G-R\cos\theta)}{\sin^2\theta} - \frac{3n^2\sin^2\gamma\sin 2\theta(I_x-I)(1+e\cos f)^3}{2I},\end{aligned} \tag{26}$$

$$\dot{\gamma} = \frac{G-R\cos\theta}{\sin^2\theta} + \frac{n(1+e\cos f)^2\cos\theta\cos\gamma}{\sin\theta}, \tag{27}$$

$$\begin{aligned}\dot{G} = \frac{n(1+e\cos f)^2\sin\gamma(G\cos\theta - R)}{\sin\theta} + n^2(1+e\cos f)^4\cos\gamma\sin\gamma\\ -\dot{\theta}n(1+e\cos f)^2\cos\gamma - \frac{3n^2\cos\gamma\sin\gamma\sin^2\theta(I_x-I)(1+e\cos f)^3}{I},\end{aligned} \tag{28}$$

$$\dot{\varphi} = \frac{R}{\overline{I}_x} - \frac{(G-R\cos\theta)\cos\theta}{\sin^2\theta} - \frac{n(1+e\cos f)^2\cos\gamma}{\sin\theta}, \tag{29}$$

where $R$=const. The angle $\varphi$ is not contained in equations (26)-(28), therefore, these equations can be integrated separately from equation (29). Using the generally accepted approach, let us pass from time to a new independent variable $f$. It also assumed that

$$R = nk^2\overline{R}, \qquad G = nk^2\overline{G}, \tag{30}$$ ,

where $k = 1+e\cos f$. After passing to a new independent variable, the equations take the form

$$
\begin{aligned}
\theta'' = &-\frac{(G - R\cos\theta)(R - G\cos\theta)}{\sin^3\theta} + \frac{L_I}{In^2k^4} + \frac{\cos^2\gamma\cos\theta}{\sin\theta} \\
&+ \frac{2\cos\gamma(\bar{G} - \bar{R}\cos\theta)}{\sin^2\theta} - \frac{3\sin^2\gamma\sin 2\theta(I_x - I)}{2Ik} + \frac{2\theta' e\sin f}{k},
\end{aligned} \tag{31}
$$

$$
\bar{G}' = \frac{k^2\sin\gamma(\bar{G}\cos\theta - \bar{R})}{\sin\theta} + k^2\cos\gamma\sin\gamma - k^2\theta'\cos\gamma - \frac{3\sin 2\gamma\sin^2\theta(I_x - I)k}{2I}, \tag{32}
$$

$$
\gamma' = \frac{\bar{G} - \bar{R}\cos\theta}{\sin^2\theta} + \frac{\cos\theta\cos\gamma}{\sin\theta}, \tag{33}
$$

In the case of circular orbit $e = 0$, $k = 1$, and equations (31)-(32) take form

$$
\begin{aligned}
\theta'' = &-\frac{(\bar{G} - \bar{R}\cos\theta)(\bar{R} - \bar{G}\cos\theta)}{\sin^3\theta} + \frac{L_I}{In^2} + \frac{\cos^2\gamma\cos\theta}{\sin\theta} \\
&+ \frac{2\cos\gamma(\bar{G} - \bar{R}\cos\theta)}{\sin^2\theta} - \frac{3\sin^2\gamma\sin 2\theta(I_x - I)}{2I},
\end{aligned} \tag{34}
$$

$$
\bar{G}' = \frac{\sin\gamma(\bar{G}\cos\theta - \bar{R})}{\sin\theta} + \cos\gamma\sin\gamma - \theta'\cos\gamma - \frac{3\sin 2\gamma\sin^2\theta(I_x - I)}{2I}, \tag{35}
$$

The equations obtained in this way describe the attitude motion of the space debris object in the case when its center of mass moves in Keplerian and circular orbits.

### 2.4 Stationary motions of symmetrical space debris

In order to find stationary motions, we consider motion of the space debris object in a circular orbit and equate the derivatives to zero: $\bar{G}' = 0$, $\theta'' = 0$, $\theta' = 0$, $\gamma' = 0$. From equation (33) it follows that

$$
\cos\gamma_* = \frac{\bar{R}\cos\theta_* - \bar{G}_*}{\cos\theta_*\sin\theta_*}, \tag{36}
$$

$$
\begin{aligned}
0 = &-\frac{(\bar{G}_* - \bar{R}\cos\theta_*)(\bar{R} - \bar{G}_*\cos\theta_*)}{\sin^3\theta_*} + \frac{L_{Iz}^{(2)}(\theta_*)}{In^2} + \frac{\cos^2\gamma_*\cos\theta_*}{\sin\theta_*} \\
&+ \frac{2\cos\gamma_*(\bar{G}_* - \bar{R}\cos\theta_*)}{\sin^2\theta_*} - \frac{3\sin^2\gamma_*\sin 2\theta_*(I_x - I)}{2I},
\end{aligned} \tag{37}
$$

$$
0 = \frac{\sin\gamma_*(\bar{G}_*\cos\theta_* - \bar{R})}{\sin\theta_*} + \cos\gamma_*\sin\gamma_* - \frac{3\sin 2\gamma_*\sin^2\theta_*(I_x - I)}{2I}, \tag{38}
$$

where the star index indicates stationary motion. Equation (38) yields

$$\frac{G_* \cos\theta_* - R}{\sin\theta_*} + \cos\gamma_* - \frac{3\sin^2\theta_* \cos\gamma_* (I_x - I)}{I} = 0\,. \tag{39}$$

another solution of this equation $\sin\gamma_* = 0$ contradicts the equation (36). Substitution of (36) into (39) gives

$$\frac{3\sin\theta_* (\bar{G}_* - \bar{R}\cos\theta_*)(I_x - I)}{I\cos\theta_*} - \frac{\bar{G}_* \sin\theta_*}{\cos\theta_*} = 0 \tag{40}$$

From here we define

$$\bar{G}_* = \frac{3\cos\theta_* \bar{R}(I_x - I)}{3I_x - 4I}\,. \tag{41}$$

From (36) and (41) it follows that

$$\cos\gamma_* = -\frac{\bar{R}I}{(3I_x - 4I)\sin\theta_*}, \tag{42}$$

Substitution of (41) and (36) into (37) yields

$$L_I(\theta_*) - 3n^2(I_x - I)\cos\theta_* \sin\theta_* = 0\,. \tag{43}$$

The last equation expresses the equality of the gravitational gradient and the ion torques. The solutions of equation (40) depend on the form of the function $L_I(\theta_*)$, which in turn depends on the shape of the body and the ion beam parameters. The solution to this nonlinear equation should be searched numerically for a specific space debris object under consideration. Depending on the view of function $L_I$, the equation (43) can have a different number of roots. Once solutions are found, the corresponding values of $\bar{G}_*$ and $\gamma_*$ can be determined from equations (41) and (42) respectively.

## 3 Space debris attitude control

It is assumed that during the motion, the spacecraft's control system keeps it in a constant position relative to the space debris $x_A = d = const$, $y_A = 0$, $z_A = 0$. The axis of the ion flow is always directed to the space debris object center of mass. To control the attitude motion of space debris, we will control the thrust of the engine that creates the ion beam. In this case, the ion torque can be defined as

$$L_I = u(\theta, \theta', G, \gamma) L_{I\max}(\theta), \tag{44}$$

where $u \in [0,1]$ is dimensionless control parameter, which is proportional to the square rate of the ions velocity and can be changed by the voltage in the thruster. The value $u = 0$ corresponds to the off engine, and the value $u = 1$ corresponds to the engine turned on at full power $L_I = L_{I\max}(\theta)$. To calculate the dependence of the ion torque $L_{I\max}$ on the angle $\theta$, an author's Matlab implementation of the computational procedure described in detail in (Alpatov et al., 2019; Aslanov and Ledkov, 2017) is used. The surface of the object blown by the ion beam is divided into triangles and the force effect of the ions on each of them is calculated. Then summation is performed.

To control the space debris attitude motion, it is proposed to use the following feedback control law, which puts the system in a stationary motion mode

$$u = \begin{cases} 0, & \text{when } \bar{u} \le 0; \\ \bar{u}, & \text{when } 0 < \bar{u} < 1; \\ 1, & \text{when } \bar{u} \ge 1; \end{cases} \tag{45}$$

where

$$\bar{u} = 1 + \left( k_\theta (\theta_* - \theta) - k_\Omega \theta' + k_\gamma (\gamma_* - \gamma) + k_G (\bar{G}_* - \bar{G}) \right) \frac{In^2 k^4}{L_{I\max}(\theta)}, \tag{46}$$

where $k_j$ are control law parameters. To determine the control law parameters, the cost function is introduced in the form

$$F(k_\theta, k_\Omega, k_\gamma, k_G) = (\theta_* - \theta_{Tav})^2 + {\theta'_{Tav}}^2 + (\gamma_* - \gamma_{Tav})^2 + (\bar{G}_* - \bar{G}_{Tav})^2, \tag{47}$$

where $\theta_{Tav}$, $\theta'_{Tav}$, $\gamma_{Tav}$, $\bar{G}_{Tav}$ are average values of the variables calculated for the last period of oscillations. To calculate this function, the system of equations (33)-(35) is numerically integrated with the specific values $k_\theta$, $k_\Omega$, $k_\gamma$, $k_G$ transferred as parameters. Integration is performed on an independent variable interval of ten periods. Then the last period is taken, and the amplitude values of the variables for this period are found. The arithmetic mean values for these amplitude values are substituted into the formula (47) as $\theta_{Tav}$, $\theta'_{Tav}$, $\gamma_{Tav}$, $\bar{G}_{Tav}$. To find a set of control parameters $k_\theta$, $k_\Omega$, $k_\gamma$, $k_G$ that ensure the minimum cost function (47), the Nelder-Mead method (Lagarias et al., 1998), which is implemented in Matlab as FMINSEARCH, is used in this study. The efficiency of using the proposed control law will be demonstrated in the next section.

## 4 Numerical simulation results

As an example, let us consider the deorbiting of a hypothetical rigid body, close in shape to the Cosmos upper stage, using an ion beam. Cases of uncontrolled and controlled motion will be compared bellow. It is assumed that space debris mass $m_B = 1400\text{kg}$, moments of inertia $I_x = 1300\,\text{kg}\cdot\text{m}^2$, $I_y = I_z = I = 6800\,\text{kg}\cdot\text{m}^2$, the length of the stage is 6m, its diameter is 2.4 m. The center of mass of the space debris lies on the axis of symmetry and is shifted to the lower end by 0.5 m. The active spacecraft mass $m_B = 450\text{kg}$. The distance between the spacecraft and space debris center of mass $d = 15\text{m}$. The ion beam axis velocity is 38000 m/s, plasma density is $2.6\cdot 10^{16}$, ion beam divergence angle is $15°$. The parameters of the ion beam were taken from report (Bombardelli et al., 2011). Figures 2 and 3 show the dependences of the ion torque and force on the angle $\theta$, which were obtained for body and ion beam with the above parameters.

At the initial moment of time, space debris center of mass has the following motion parameters: $r_{B0} = 6671000\text{m}$, $\dot{r}_{B0} = 0$, $\dot{f}_0 = 1.1587\cdot 10^{-3}\text{rad/s}$. These values correspond to $n = 1.1587\cdot 10^{-3}\text{rad/s}$, $e = 0$. Let us take $\omega_x^b = 0.0005\text{rad/s}$, $\omega_y^b = 0.02\text{rad/s}$, $\omega_z^b = 0.03\text{rad/s}$, for which according (15) and (30) $\bar{G} = 0.0803$, and $\bar{R} = 0.0825$.

Let us find stationary values. Numerical solution of equation (43) gives the following roots: $\theta_{*1} = 0$, $\theta_{*2} = 1.9324\text{rad}$, $\theta_{*3} = \pi$, $\theta_{*4} = 4.3508\text{rad}$, $\theta_{*5} = 2\pi$. Modeling shows that roots with odd indices correspond to unstable equilibrium, and roots with even indices are stable equilibrium. Let us choose the second root as a stationary position to which we will stabilize the oscillations: $\theta_* = \theta_{*2}$. Equations (41) and (42) give the following results for this value: $\bar{G}_* = -2.0668 \cdot 10^{-2}$, $\gamma_* = 1.5451\text{rad}$.

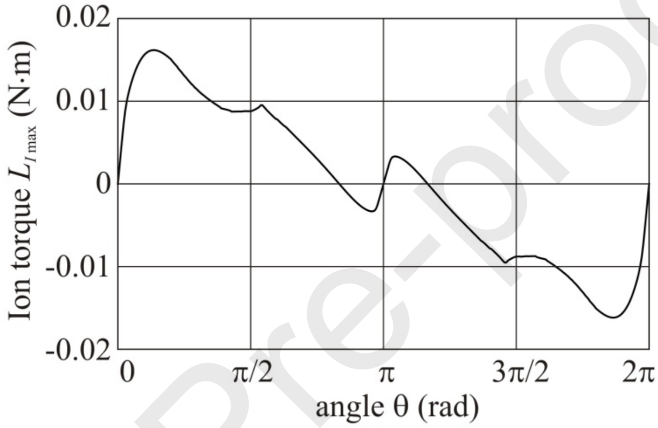


Fig. 2. Dependence of ion beam torque $L_{I\max}$ on angle $\theta$

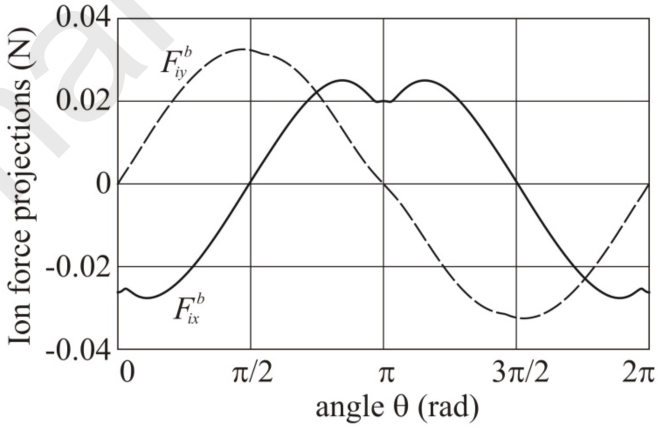


Fig. 3. Dependence of ion beam force projections $F_{ix}^b$, $F_{iy}^b$ on angle $\theta$

Let at the initial moment of time $\theta_0 = 2.2\text{rad}$, $\gamma_0 = 1.7\text{rad}$, $\bar{G} = 0.0803$. Let us simulate the motion of the system using the control law (45) . The minimization of the cost function (47) using FMINSEARCH function in Matlab gives the following values of the control law parameters: $k_\theta = 16.7469$, $k_\Omega = 8.3178$, $k_G = 12.3538$, $k_\gamma = 43.9145$. Figures 4-6 show the graphs obtained in the case of uncontrolled motion and when using the proposed control law.

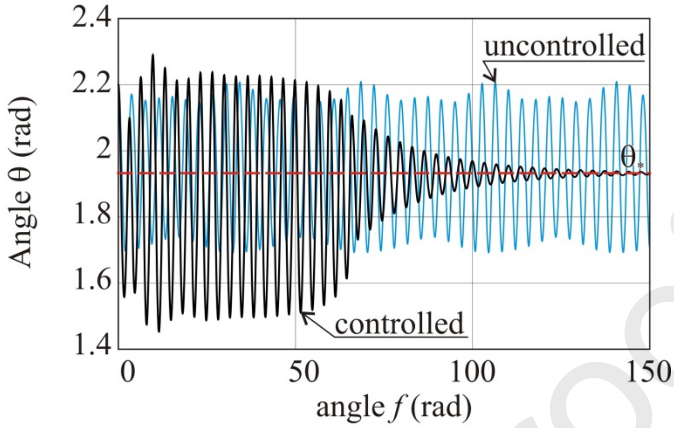


Fig. 4. Dependence of angle $\theta$ on angle $f$.

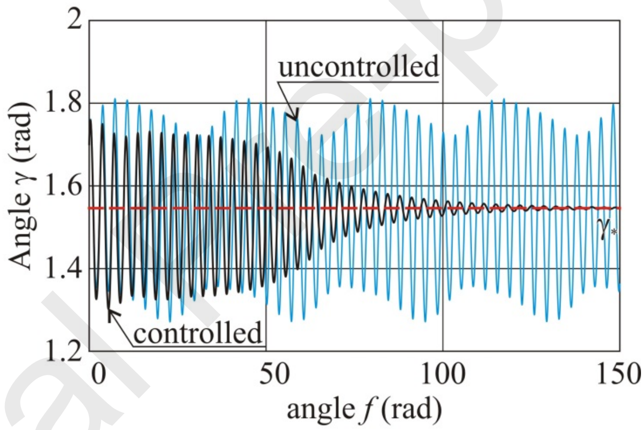


Fig. 5. Dependence of angle $\gamma$ on angle $f$.

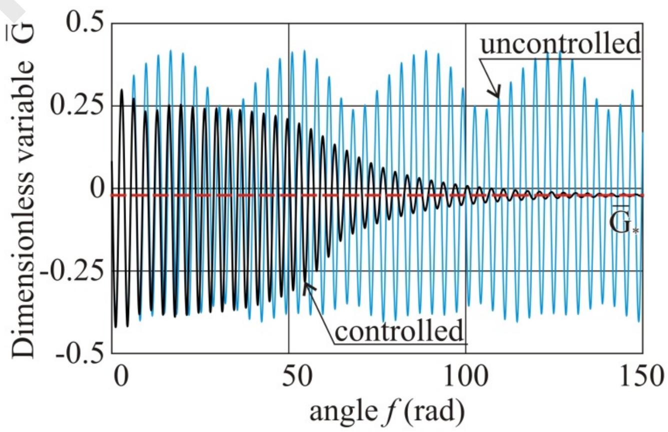


Fig. 6. Dependence of $\overline{G}$ on angle $f$.

The dependence of the dimensionless function of the control law $u$ on the angle $f$ is shown in Figure 7. The figure shows that at the initial stage, the control has a close to relay character, but as the system parameters approach the stationary position, the control takes the form of a nonlinear function bounded from above (when $f > 66.14\text{rad}$). At $u$=1 and $u$=0, the control remains continuous, but not smooth.

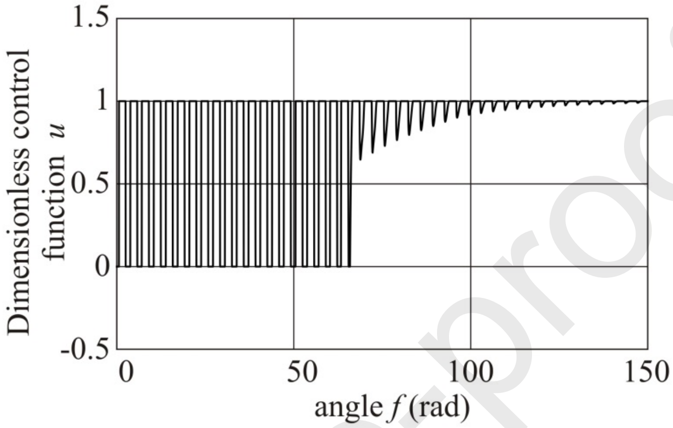


Fig. 7. Dependence of control function (45) on angle $f$.

Analysis of the graphs of controlled motion allows to hypothesize that the found stationary position $\theta_*$, $\bar{G}_*$, $\gamma_*$ is asymptotically stable. For a strictly mathematical proof of this hypothesis, a rougher study using the Lyapunov's theory is required. Since the control (45) is a continuous piecewise non-smooth function, the derivative of which is not defined at the switching points, the direct use of classical Lyapunov's theorems is impossible, and the use of the theory of differential inclusions is required (Leine and Nijmeijer, 2013). This issue will be the topic of our future research. Here we will focus on the numerical analysis of the mechanical system behavior. A series of numerical calculations with different initial conditions was carried out to determine the region of attraction of this equilibrium. It is difficult to visualize the surface that bounds the region of attraction in four-dimensional space ($\theta$, $\gamma$, $\theta'$, $\bar{G}$). Figures 8 and 9 show two cross sections. Figure 8 was built for constant values $\theta_0' = 0$, $\bar{G}_0 = \bar{G}_*$, and Figure 9 was built for $\theta_0 = \theta_*$, $\gamma_0 = \gamma_*$. The gray points in Figures 8 and 9 correspond to the initial conditions for which the phase trajectory passes into the vicinity of the stationary position at an interval of 500 rad.

According to the data given in the study (Šilha et al., 2018), the angular velocities of the rocket stages can reach values of 409.6 deg/s. Using equations (16), it can be shown that the modulus of angular velocity inside the region of attraction, which is shown in Figure 9, does not exceed 0.0034 rad/s. Thus, the proposed control can be used to stabilize slowly rotating objects.

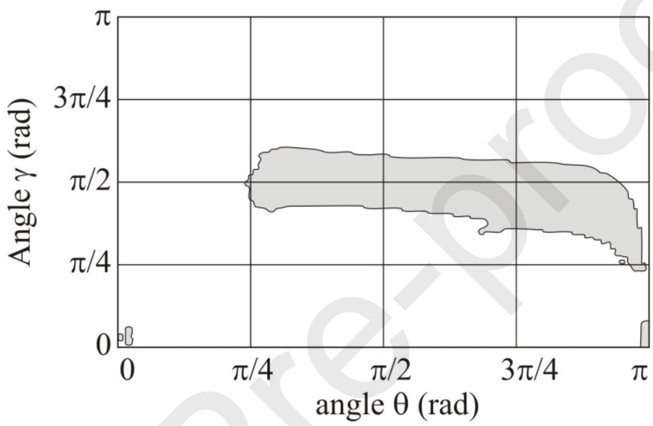


Fig. 8. The region of attraction of stationary position in ($\theta$, $\gamma$) space .

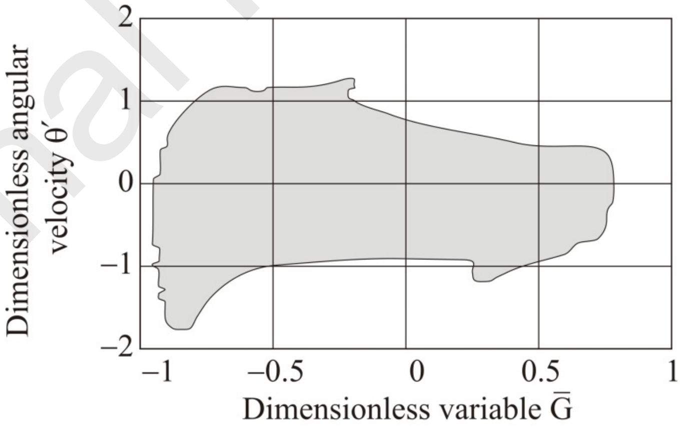


Fig. 9. The region of attraction of stationary position in ($\bar{G}$, $\theta'$) space.

Calculations show that the proposed control law can be used for weakly elliptical orbits. Figure 10 shows the dependence of angle $\theta$ on angle $f$ for various values of the eccentricity. Figures 11 and 12 show the change in angle $\gamma$ and dimensionless variable $\bar{G}$ respectively.

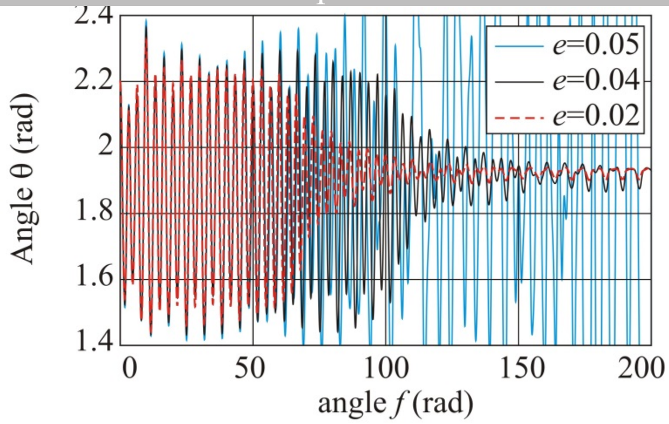


Fig. 10. Dependence of angle $\theta$ on angle $f$ for various eccentricities.

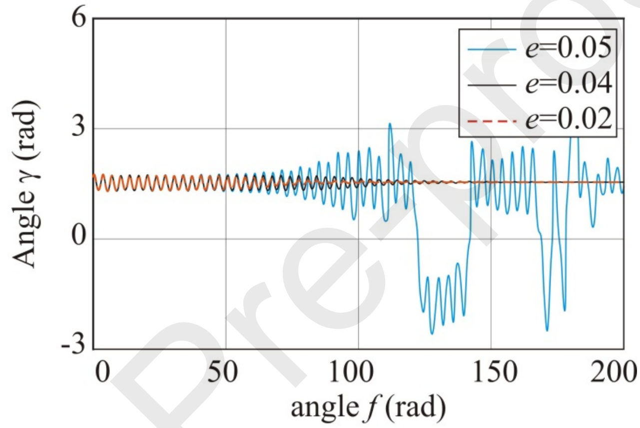


Fig. 11. Dependence of angle $\gamma$ on angle $f$ for various eccentricities.

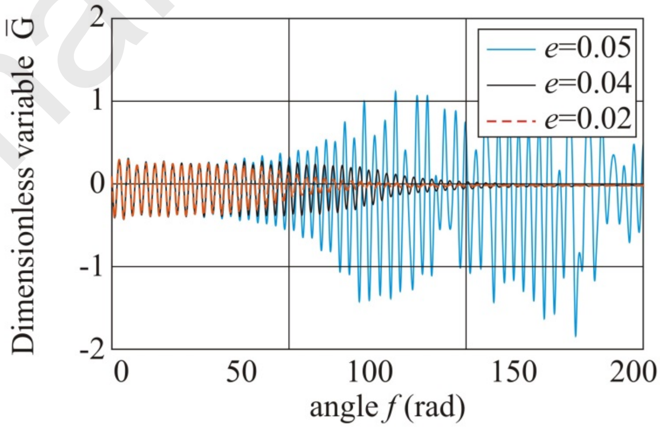


Fig. 12. Dependence of $\bar{G}$ on angle $f$ for various eccentricities.

It can be seen that at the eccentricity value of 0.04, the control law copes with the task, and the variables approach the stationary values. With an eccentricity value of 0.05, the control is ineffective and rather leads to a buildup of the system. This is due to the narrowing of the region of attraction of an asymptotically stable equilibrium position as a result of an increase in perturbations associated with a change in the gravitational moment in an elliptical orbit. Moreover, the equilibrium position itself is impossible in an elliptical orbit. Instead of a position of equilibrium, the phase trajectories are attracted to a stable limit cycle, which is closed trajectory in phase space. Limit cycle projections on planes for various eccentricities are shown in Figures 13 and 14. To obtain these graphs, the numerical integration of the equations of motion (31)-(35) over a large interval ($f \in [0, 2500]$ rad) was performed, and then the last period was plotted.

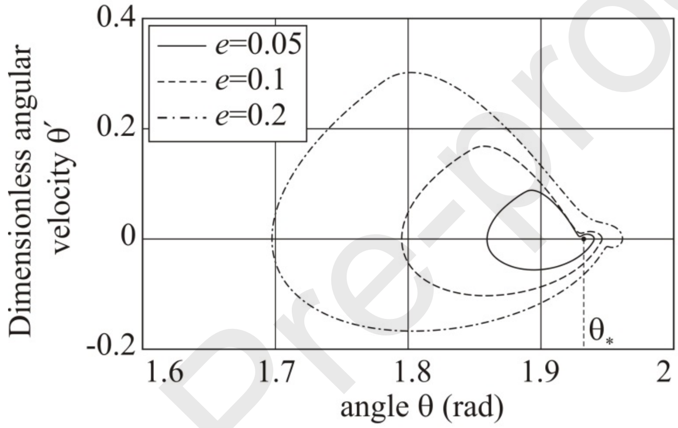


Fig. 13. Stable limit cycles for various eccentricities in ($\theta$, $\theta'$) space.

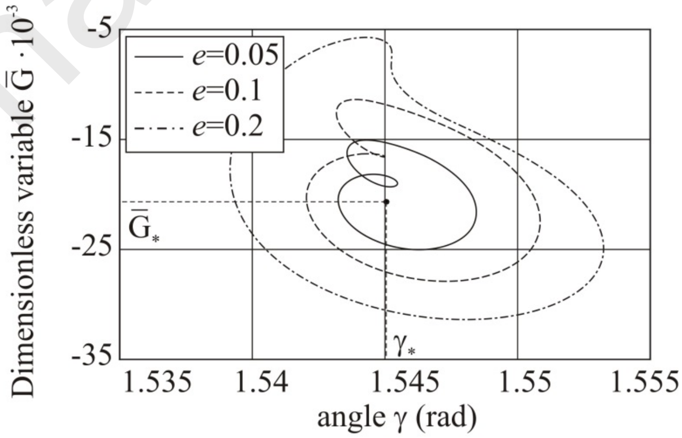


Fig. 14. Stable limit cycles for various eccentricities in ($\gamma$, $\bar{G}$) space.

Calculations have shown that in the case of nonzero eccentricity the control parameters $k_\theta$, $k_\Omega$, $k_\gamma$, $k_G$, which provide a minimum to cost function (47), change, but insignificantly. This refinement does not lead to a qualitative change in the observed behavior, but requires significant computational costs. Therefore, for the purpose of optimization, it was decided to carry out calculations with the values of the control coefficients obtained for a circular orbit. When preparing real missions, more accurate and resource-intensive calculations, without this simplification, must be performed.

## Conclusion

The paper considers the contactless transportation of space debris by means of an ion beam generated by the electrodynamic engine of an active spacecraft. A mathematical model describing the motion of a mechanical system consisting of an active spacecraft, which is considered as a material point, and a dynamically symmetric object of space debris in the shape of a cylinder, was built. Quantities proportional to the generalized momentum corresponding to rotation and precession angles in the classical Lagrange case of rigid body motion, which are named R-G variables here, were used as system variables instead of angular velocities. A simplified mathematical model describing space debris attitude motion in the case when its center of mass moves in a Keplerian orbit. Stationary solutions for the case of motion in a circular orbit were found. A feedback control law that stabilizes the angular oscillations of a space debris object in a stationary position was proposed. Numerical simulation has shown that the proposed law can be used in orbits with small eccentricities when the object rotates at a low angular velocity. This work is the first attempt to study the controlled spatial motion of space debris within the framework of the ion beam shepherd concept. The results of the work can be used in the development of space debris removal missions.

**Acknowledgments**

This study was supported by the Russian Science Foundation (Project No. 19-19-00085).

# Appendix

The rotation matrices that were used to derive the equations of motion are given here. Transformation from planetocentric frame $OX_pY_pZ_p$ to orbital frame $BX_oY_oZ_o$ can be performed by two rotations: the positive rotation around the axis $OY_p$ on the angle $f$, and the negative rotation around the axis $OX_o$ on the angle $\nu$. These rotations are given by matrices $\mathbf{M}_{1p}$ and $\mathbf{M}_{o1}$, respectively

$$\mathbf{M}_{1p} = \begin{bmatrix} \mathrm{c}_f & 0 & -\mathrm{s}_f \\ 0 & 1 & 0 \\ \mathrm{s}_f & 0 & \mathrm{c}_f \end{bmatrix}, \quad \mathbf{M}_{o1} = \begin{bmatrix} 1 & 0 & 0 \\ 0 & \mathrm{c}_\nu & -\mathrm{s}_\nu \\ 0 & \mathrm{s}_\nu & \mathrm{c}_\nu \end{bmatrix},$$

where $c_\alpha = \cos\alpha$, $s_\alpha = \sin\alpha$. The rotation matrix $\mathbf{M}_{op}$ can be defined as

$$\mathbf{M}_{op} = \mathbf{M}_{o1}\mathbf{M}_{1p} = \begin{bmatrix} \mathrm{c}_f & 0 & -\mathrm{s}_f \\ -\mathrm{s}_f\,\mathrm{s}_\nu & \mathrm{c}_\nu & -\mathrm{c}_f\,\mathrm{s}_\nu \\ \mathrm{s}_f\,\mathrm{c}_\nu & \mathrm{s}_\nu & \mathrm{c}_f\,\mathrm{c}_\nu \end{bmatrix},$$

The inverse transition can be made using the matrix $\mathbf{M}_{po} = \mathbf{M}_{op}^{-1} = \mathbf{M}_{op}^{T}$.

The transition from the orbital to the body coordinate system can be accomplished in three Euler rotations x-z-x. The first rotation around the axis $BX_o$ on the angle $\gamma$ is transfers the axes $BX_oY_oZ_o$ to the axes $BX_oY_2Z_2$. It is defined by the matrix $\mathbf{M}_{2o}$. The second rotation around the axis $BZ_2$ on the angle $\theta$ is transfers the axes $BX_oY_2Z_2$ to the axes $BX_bY_3Z_2$. It is defined by the matrix $\mathbf{M}_{32}$. The third rotation around the axis $BX_b$ on the angle $\varphi$ is transfers the axes $BX_bY_3Z_2$ to the axes $BX_bY_bZ_b$. It is defined by the matrix $\mathbf{M}_{b3}$. The rotation matrixes are

$$\mathbf{M}_{2o} = \begin{bmatrix} 1 & 0 & 0 \\ 0 & \mathrm{c}_\gamma & \mathrm{s}_\gamma \\ 0 & -\mathrm{s}_\gamma & \mathrm{c}_\gamma \end{bmatrix}, \quad \mathbf{M}_{32} = \begin{bmatrix} c_\theta & s_\theta & 0 \\ -s_\theta & \mathrm{c}_\theta & 0 \\ 0 & 0 & 1 \end{bmatrix}, \quad \mathbf{M}_{b3} = \begin{bmatrix} 1 & 0 & 0 \\ 0 & \mathrm{c}_\varphi & \mathrm{s}_\varphi \\ 0 & -\mathrm{s}_\varphi & \mathrm{c}_\varphi \end{bmatrix}.$$

Transformation from orbital to body frame can be defined by rotation matrix

$$\mathbf{M}_{bo} = \begin{bmatrix} c_\theta & s_\theta c_\gamma & s_\theta s_\gamma \\ -\mathrm{c}_\varphi \mathrm{s}_\theta & c_\varphi c_\theta c_\gamma - s_\varphi s_\gamma & c_\varphi c_\theta s_\gamma + s_\varphi c_\gamma \\ s_\varphi \mathrm{s}_\theta & -s_\varphi c_\theta c_\gamma - c_\varphi s_\gamma & -s_\varphi c_\theta s_\gamma + c_\varphi c_\gamma \end{bmatrix}.$$

The inverse transition can be made using the matrix $\mathbf{M}_{ob} = \mathbf{M}_{bo}^{-1} = \mathbf{M}_{bo}^{T}$.

## References


Alpatov, A., Khoroshylov, S., Bombardelli, C., 2018. Relative control of an ion beam shepherd satellite using the impulse compensation thruster. Acta Astronaut. 151, 543–554. https://doi.org/10.1016/j.actaastro.2018.06.056

Alpatov, A.P., S.V. Khoroshylov, S.V., Maslova, A.I., 2019. Contactless de-orbiting of space debris by the ion beam. Dynamics and Control. Akademperiodyka, Kyiv. https://doi.org/10.15407/akademperiodyka.383.170

Aslanov, V., Ledkov, A., Konstantinov, M., 2020. Chaotic motion of a cylindrical body during contactless transportation from MEO to LEO by ion beam. Nonlinear Dyn. 101, 1221–1231. https://doi.org/10.1007/s11071-020-05822-0

Aslanov, V.S., 2019. Debris removal in GEO by heavy orbital collector. Acta Astronaut. 164, 184–191. https://doi.org/10.1016/j.actaastro.2019.07.021

Aslanov, V.S., 2017. Rigid Body Dynamics for Space Applications. Elsevier.

Aslanov, V.S., 2016. Swing principle for deployment of a tether-assisted return mission of a re-entry capsule. Acta Astronaut. 120, 154–158. https://doi.org/10.1016/j.actaastro.2015.12.020

Aslanov, V.S., Ledkov, A.S., 2020. Space debris attitude control during contactless transportation in planar case. J. Guid. Control. Dyn. 43, 451–461. https://doi.org/10.2514/1.G004686

Aslanov, V.S., Ledkov, A.S., 2017. Attitude motion of cylindrical space debris during its removal by ion beam. Math. Probl. Eng. 2017. https://doi.org/10.1155/2017/1986374

Baranov, A.A., Grishko, D.A., Shcheglov, G.A., Sholmin, A.S., Stognii, M.V., Kamenev, N.D., 2021. Feasibility analysis of LEO and GEO large space debris de/re-orbiting taking into account launch mass of spacecraft-collector and its configuration layout. Adv. Sp. Res. 67, 371–383. https://doi.org/10.1016/j.asr.2020.09.005

Bennett, T., Schaub, H., 2018. Contactless electrostatic detumbling of axi-symmetric GEO objects with nominal pushing or pulling. Adv. Sp. Res. 62, 2977–2987. https://doi.org/10.1016/j.asr.2018.07.021

Bombardelli, C., Merino-Martinez, M., Galilea, E., Palaez, J., Urrutxua, H., Herrara-Montojo, J., Iturri-Torrea, A., 2011. Ariadna Call for Ideas: Active Removal of Space Debris. Ion Beam Shepherd for Contactless Debris Removal.

Bombardelli, C., Peláez, J., 2011. Ion beam shepherd for contactless space debris removal. J. Guid. Control. Dyn. 34, 916–920. https://doi.org/10.2514/1.51832

Bonnal, C., Alby, F., 2000. Measures to reduce the growth or decrease the space debris population. Acta Astronaut. 47, 699–706. https://doi.org/10.1016/S0094-5765(00)00107-7

Cichocki, F., Merino, M., Ahedo, E., Smirnova, M., Mingo, A., Dobkevicius, M., 2017. Electric propulsion subsystem optimization for “ion Beam Shepherd” missions. J. Propuls. Power 33, 370–378. https://doi.org/10.2514/1.B36105

Hakima, H., Emami, M.R., 2021. Deorbiter CubeSat mission design. Adv. Sp. Res. 67, 2151–2171. https://doi.org/10.1016/j.asr.2021.01.005

Ivakin, S., Avdeev, A., Boreysho, A., Katorgin, B., Metelnikov, A., 2019. Nuclear powered spaceborne laser for orbital debris removal, in: Di Lazzaro, P. (Ed.), XXII International Symposium on High Power Laser Systems and Applications. SPIE, pp. 1–6. https://doi.org/10.1117/12.2522456

Kessler, D.J., Cour-Palais, B.G., 1978. Collision frequency of artificial satellites: The creation of a debris belt. J. Geophys. Res. 83, 2637. https://doi.org/10.1029/JA083iA06p02637

Khoroshylov, S., 2020. Relative control of an ion beam shepherd satellite in eccentric orbits. Acta Astronaut. 176, 89–98. https://doi.org/10.1016/j.actaastro.2020.06.027

Kitamura, S., 2010. Large space debris reorbiter using ion beam irradiation, in: 61 St International Astronautical Congress, Prague, Czech Republic.

Kitamura, S., Hayakawa, Y., Kawamoto, S., 2014. A reorbiter for large GEO debris objects using ion beam irradiation. Acta Astronaut. 94, 725–735. https://doi.org/10.1016/j.actaastro.2013.07.037

Klinkrad, H., Beltrami, P., Hauptmann, S., Martin, C., Sdunnus, H., Stokes, H., Walker, R., Wilkinson, J., 2004. The ESA Space Debris Mitigation Handbook 2002. Adv. Sp. Res. 34, 1251–1259. https://doi.org/10.1016/j.asr.2003.01.018

Lagarias, J.C., Reeds, J.A., Wright, M.H., Wright, P.E., 1998. Convergence properties of the Nelder-Mead simplex method in low dimensions. SIAM J. Optim. 9, 112–147.

Leine, R.I., Nijmeijer, H., 2013. Dynamics and bifurcations of non-smooth mechanical systems. Springer Science.

Letizia, F., Lemmens, S., Bastida Virgili, B., Krag, H., 2019. Application of a debris index for global evaluation of mitigation strategies. Acta Astronaut. 161, 348–362. https://doi.org/10.1016/j.actaastro.2019.05.003

Maclay, T., McKnight, D., 2021. Space environment management: Framing the objective and setting priorities for controlling orbital debris risk. J. Sp. Saf. Eng. 8, 93–97. https://doi.org/10.1016/j.jsse.2020.11.002

Mark, C.P., Kamath, S., 2019. Review of Active Space Debris Removal Methods. Space Policy 47, 194–206. https://doi.org/10.1016/j.spacepol.2018.12.005

Nakajima, Y., Tani, H., Yamamoto, T., Murakami, N., Mitani, S., Yamanaka, K., 2018. Contactless space debris detumbling: A database approach based on computational fluid dynamics. J. Guid. Control. Dyn. 41, 1906–1918. https://doi.org/10.2514/1.G003451

NASA, 2021. Orbital Debris Quarterly News. Natl. Aeronaut. Sp. Adm. 25, 1–12.

Obukhov, V.A., Kirillov, V.A., Petukhov, V.G., Popov, G.A., Svotina, V. V, Testoyedov, A., Usovik, I. V, 2021. Acta Astronautica Problematic issues of spacecraft development for contactless removal of space debris by ion beam. Acta Astronaut. 1–10. https://doi.org/10.1016/j.actaastro.2021.01.043

Pardini, C., Anselmo, L., 2020. Environmental sustainability of large satellite constellations in low earth orbit. Acta Astronaut. 170, 27–36. https://doi.org/10.1016/j.actaastro.2020.01.016

Pardini, C., Anselmo, L., 2011. Physical properties and long-term evolution of the debris clouds produced by two catastrophic collisions in Earth orbit. Adv. Sp. Res. 48, 557–569. https://doi.org/10.1016/j.asr.2011.04.006

Peltoniemi, J.I., Wilkman, O., Gritsevich, M., Poutanen, M., Raja-Halli, A., Näränen, J., Flohrer, T., Di Mira, A., 2021. Steering reflective space debris using polarised lasers. Adv. Sp. Res. 67, 1721–1732. https://doi.org/10.1016/j.asr.2021.01.002

Popov, G., Aslanov, V., Petukhov, V., Ledkov, A., 2020. Influence of space debris attitude motion on ion beam assisted removal mission costs, in: Proceedings of the International Astronautical Congress, IAC. International Astronautical Federation, IAF, pp. 1–7.

Rossi, A., Valsecchi, G.B., Alessi, E.M., 2015. The criticality of spacecraft index. Adv. Sp. Res. 56, 449–460. https://doi.org/10.1016/j.asr.2015.02.027

Schaub, H., Junkins, J.L., 2014. Analytical Mechanics of Space Systems, Third Edition, Analytical Mechanics of Space Systems, Third Edition. American Institute of Aeronautics and Astronautics, Inc., Washington, DC. https://doi.org/10.2514/4.102400

Schaub, H., Moorer, D.F., 2012. Debris Reorbiter : Challenges and Prospects. J. Astronaut. Sci. 59, 165–180.

Shan, M., Guo, J., Gill, E., 2016. Review and comparison of active space debris capturing and removal methods. Prog. Aerosp. Sci. 80, 18–32. https://doi.org/10.1016/j.paerosci.2015.11.001

Šilha, J., Pittet, J.-N., Hamara, M., Schildknecht, T., 2018. Apparent rotation properties of space debris extracted from photometric measurements. Adv. Sp. Res. 61, 844–861. https://doi.org/10.1016/j.asr.2017.10.048

Urrutxua, H., Bombardelli, C., Hedo, J.M., 2019. A preliminary design procedure for an ion-beam shepherd mission. Aerosp. Sci. Technol. 88, 421–435.

Yu, Y., Yang, F., Yue, H., Lu, Y., Li, S., Zhao, H., 2021. Prospects of de-tumbling large space debris using a two-satellite electromagnetic formation. Adv. Sp. Res. 67, 1816–1829. https://doi.org/10.1016/j.asr.2020.12.039

Zhong, R., Zhu, Z.H., 2016. Timescale separate optimal control of tethered space-Tug systems for space-debris removal. J. Guid. Control. Dyn. 39, 2539–2544. https://doi.org/10.2514/1.G001867

Highlights:

- Simplified mathematical model describing 3D motion of dynamically symmetric space debris relative its center of mass in Keplerian orbit under the influence of the ion beam.
- Equation of stationary motion of space debris in a circular orbit under the action of an ion beam.
- A feedback control law that stabilizes the 3D angular oscillations of a space debris object in a stationary position.

## Declaration of interests

☒ The authors declare that they have no known competing financial interests or personal relationships that could have appeared to influence the work reported in this paper.

☐The authors declare the following financial interests/personal relationships which may be considered as potential competing interests: